Fast assessment of structural models of ion channels based on their predicted current-voltage characteristics

Witold Dyrka, Monika Kurczynska, Bogumil M. Konopka, Malgorzata Kotulska

June 23, 2015

Department of Biomedical Engineering, Wroclaw University of Technology,
Wybrzeze Wyspianskiego 27, 50-370 Wroclaw, Poland

E-mail: {witold.dyrka, monika.kurczynska, bogumil.konopka, malgorzata.kotulska}@pwr.wroc.pl

Running title: Function-oriented MQAP for ion channels

Abstract

Computational prediction of protein structures is a difficult task, which involves fast and accurate evaluation of candidate model structures. We propose to enhance single model quality assessment with a functionality evaluation phase for proteins whose quantitative functional characteristics are known. In particular, this idea can be applied to evaluation of structural models of ion channels, whose main function - conducting ions - can be quantitatively measured with the patch-clamp technique providing the current-voltage characteristics. The study was performed on a set of KcsA channel models obtained from complete and incomplete contact maps. A fast continuous electrodiffusion model was used for calculating the current-voltage characteristics of structural models. We found that the computed charge selectivity and total current were sensitive to structural and electrostatic quality of models. In practical terms, we show that evaluating predicted conductance values is an appropriate method to eliminate modes with an occluded pore or with multiple erroneously created pores. Moreover, filtering models on the basis of their predicted charge selectivity results in a substantial enrichment of the candidate set in highly accurate models. In addition to being a proof of the concept, our function-oriented single model quality assessment tool can be directly applied for evaluation of structural models of strongly-selective protein channels. Finally, our work raises an important question whether a computational validation of functionality should not be included in the evaluation process of structural models, whenever possible.

Keywords: structure - function relationship, protein structure prediction, MQAP, Poisson-Nernst-Planck model, contact map

1 Background

Currently there are over 48 million of protein sequences stored in the resources of the Uniprot Consortium, while only 109 000 structures are deposited in the Protein Data Bank (PDB) [1], and the gap is constantly increasing. Computational methods for protein structure prediction are believed to be able to solve this problem. These methods may help to identify and counteract causes of various pathological processes through computational drug design [2, 3], drug target identification [4], and protein design [5].

Computational prediction of protein structures is a difficult task, which also involves fast and accurate evaluation of candidate model structures. The ultimate verification of quality of a protein model requires availability of the native structure, or at least of its close homologs. Typically, the assessment is based on deviations between positions of equivalent atoms in the native protein structure and in the assessed model. Classical methods include the Root Mean Square Deviation (RMSD) or Global Distance Test (GDT) used in the Critical Assessment of protein Structure Prediction competition (CASP) [6]. There are also other methods, which express structural dissimilarity between structures, combining global and local measures or considering only some of distances [7, 8, 9, 10, 11, 12, 13].

In real life situations native structures are often not attainable, which makes model evaluation a challenge. To resolve it, numerous Model Quality Assessment Programs (MQAPs), which estimate the quality of produced models and select the best predictions, have been proposed. MQAPs can be divided into three main groups: single-model, quasi single-model, and consensus methods. Consensus methods (also known as clustering methods) rank models in an ensemble in order to provide relative quality scores [14, 15, 16]. Quasi single-model class include methods which evaluate a model against structural templates [17, 18]. Finally, single-model methods (often referred to as *true MQAPs*) predict similarity between a single model and the unknown native structure based on a wide range of structure- and sequence-based features of assessed models, such as solvent accessible area, secondary structure, residue and atom contact maps, evolutionary information, statistical potentials [19, 20, 21]. The CASP10 experiment showed that consensus MQAPs outperformed single and quasi single-model methods in case of easy and moderate targets, however in case of difficult, free modeling targets without known homologs, the chances were even. One of the main reasons for developing new single and quasi single-model methods is that the consensus methods are unable to detect low quality models if the whole ensemble of models consists solely of low quality structures. Moreover the

ability of consensus methods to select the best models in groups of similar structures is limited.

In this work we propose to enhance single model assessment with a functionality evaluation phase for proteins whose quantitative functional characteristics are known. This approach can yield useful knowledge showing whether a protein model is functionally correct, which is complementary to the typical assessment based on structural features. The main difficulty is efficient measuring and modeling the functionality. It needs to be an experimentally measurable property that is sensitive to structural details of a molecule. At the same time, a modeling method needs to be fast enough to efficiently score hundreds of structural models.

Here, we apply this idea to evaluation of structural models of ion channels. The main function of these proteins is conducting ions, which can be quantitatively measured with the patch-clamp technique providing current-voltage (I-V) characteristics of a single channel [22]. Thus, current-voltage characteristics can be used as a benchmark functionality for the structural model assessment. In principle, calculation of complete I-V curve resulting from a model structure can be performed with Molecular Dynamics (MD; [23, 24]), which treats the pore and ions in a fully discrete way, or with Brownian Dynamics (BD; [25, 26]), which treats the pore and the solute in a continuous manner and the ions discretely. However, both methods are computationally expensive and thus slow. Especially MD is inappropriate for prediction of the current. The alternative is the 3-Dimensional Poisson-Nernst-Planck flow model (3D PNP), a continuous steady-state theory, in which ions are represented by their position-dependent average concentrations [27, 28, 29]. 3D PNP is less accurate than MD and BD methods but manyfold faster, typically 3-5 CPU minutes for one channel structure [30]. While, due to its simplicity, the classical 3D PNP is generally not suitable to model complex physical phenomena, it has been shown to be capable of accounting for effects of single point mutations and of predicting I-V characteristics of the quality sufficiently good for a MQAP [31, 30].

In this study, we apply the computationally enhanced 3D PNP model [29] as a function-oriented single-model MQAP on a set of structural models of the KcsA ion channel. First, models of diverse quality are obtained from complete and incomplete contact maps. Then, relations between channel structural and functional features are investigated. Finally, the predictive power of selected functional characteristics is assessed.

2 Materials and Methods

KcsA is a relatively well-studied potassium channel for which experimentally solved structure in the open-conductive configuration is available in the PDB under accession number 3FB8. It is relatively small – its transmembrane domain consists of 4 identical units of 87 amino acids each. Patch-clamp measurements at $\pm 100\,\mathrm{mV}$ revealed relatively high conductance from 57 to 75 pS, mild outward rectification (1.29) and infinite cation to anion selectivity [32] (Tab. 1).

In order to generate a set of models of diverse quality, the experimental structure 3FB8 was reduced to contact maps of information completeness varying from 30% to 100%. Then, spatial coordinates were reconstructed from the contact maps using *C2S_pipeline*, which applies several state-of-the-art bioinformatic tools [33]. Structural quality of a reconstructed model was measured using overall and single amino acid RMSD related to the original PDB structure, the diameter of entrance to the selectivity filter (SF) and deviation of oxygen atoms in SF.

The electrostatics of channel models was calculated using the Poisson-Boltzmann method and the ion flux was computed using the classical 3D PNP model. The current-voltage characteristics were quantified at external voltage of ±100 mV using plain values and absolute deviations of the inward and outward current (or equivalent conductances), inward and outward charge selectivity (i.e. ratio of cation to anion current) and rectification of the current. When applied to the reference structure, the electrodiffusion model properly predicted outward rectification of the channel and virtually infinite cation to anion selectivity (above 100:1) while total currents were underestimated 3-4-fold (Tab. 1) [30].

2.1 Computational pipeline

Our in-house software was used to generate a contact map (CMAP) based on the PDB file. A CMAP was a square matrix of -1, 0 and 1. A pair of residues was assumed to be in contact if Ca atoms of both residues were within 12 Å of one another. This distance was previously reported as the optimal contact distance for a CMAP-based protein reconstruction [34]. Remaining pairs were attributed a status of non-contact in the CMAP. In order to obtain models of different qualities CMAPs reduced to 90%, 70% 50%, and 30% of information were also generated. CMAP reduction was conducted by substituting the specified percentage of randomly selected contacts and the same percentage of non-contacts with the status of "unknown". The selection was conducted with the uniform distribution, therefore equal portions of information on contact sites were lost in all parts of the structure.

Spatial coordinates of a channel were reconstructed from the contact map in a three step procedure *C2S_pipeline*, which applied several state-of-the-art bioinformatic tools [33]. Coordinates of Cα atoms were estimated based on constraints imposed by the contact map using FT-COMAR [35, 36]. The protein backbone was reconstructed by SABBAC [37] and side-chains were added using SCWRL [38]. The protocol was adapted for modeling multimeric symmetric proteins (see [33]). The structural quality of constructed models was measured using the following features:

- Full model RMSD related to the original PDB structure,
- Model C_α-C_β RMSD related to the original PDB structure,
- RMSD of each model amino acid related to the original structure,
- Diameter of the selectivity filter (SF),
- Deviation of the selectivity filter oxygen atom, related to the original structure.

Two types of functional characteristics were calculated for each reconstructed protein structure: the electrostatic profile at the pore axis, and the current-voltage characteristics. The channel was fitted in the 129x129x129 grid at the 1 Å resolution for the Poisson-Boltzman calculations using Adaptive Poisson-Boltzmann Solver (APBS; [39]). Electrostatic profiles were obtained in absence of ions and at no external voltage. Correctness of the electrostatic profile was quantified using the Root Mean Square Error (RMSE) in reference to the profile calculated for the original channel.

Current-voltage characteristics were determined with 3D PNP Solver using the grids obtained from APBS. The dielectric constants were assumed as $\epsilon = 4$ for the protein and $\epsilon = 80$ for the solute. PNP calculations were carried under parametrization optimized for narrow channels (see [30]), including grid spacing $\Delta = 2$ Å, partition coefficient $\xi = 0.4$, dielectric constant in the pore $\epsilon = 40$ and *sphere unified* model for determining pore-radius dependent diffusion coefficient. Computational results obtained from 3D PNP Solver on the native channel structure were used as the reference characteristics for assessment of predicted models. The current-voltage characteristics were quantified at external voltage of ±100 mV using the following functional features:

- Currents
  - inward and outward cationic currents (I^+_{in}, I^+_{out}),
  - inward and outward anionic currents (I^-_{in}, I^-_{out}),
  - inward and outward (total) currents (I_{in}, I_{out});
- Inward and outward charge selectivities (i.e. ratio of cation to anion current: $I^+_{in}/I^-_{in}, I^+_{out}/I^-_{out}$);

- Rectifications of
  - cationic current ($|I^+_{out}/I^+_{in}|$),
  - anionic current ($|I^-_{out}/I^-_{in}|$),
  - (total) current ($|I_{out}/I_{in}|$).

Note that currents can be easily converted to conductance:

$$G = |I/V|,$$

where V is the electric potential applied to the membrane. The equivalence of the current and conductance is often utilized in the following of the document.

In addition to the plain values of the currents, selectivities and rectification, their deviations from the current, selectivity and rectification - calculated for the original protein structure - were also calculated. The deviation of current was calculated as a difference:

$$\Delta I = I_{model} - I_{reference},$$

The deviation of charge selectivity, and the deviation of rectification were calculated as a natural logarithm of a quotient:

$$\Delta(I^+/I^-) = \left| ln \frac{I^+_{model}/I^-_{model}}{I^+_{reference}/I^-_{reference}} \right|,$$

$$\Delta(I_{out}/I_{in}) = \left| ln \frac{|I_{out:model}/I_{in:model}|}{|I_{out:reference}/I_{in:reference}|} \right|.$$

Note that wherever the term "deviation" is used throughout this document, it always refers to the absolute deviation.

Dependencies between structural and functional features were evaluated in terms of Kendall's τ rank correlation coefficient [40].

Datasets with calculated values of functional and structural features, and with Kendall's τ and p-values for their correlations, are available as supplemental data (see Supplemental information 1).

2.2 Criteria of functional validity

Current-voltage characteristics obtained for the KcsA open-state conducting structure (PDB: 3FB8) using 3D PNP Solver in our previous work [30] were used to determine criteria for functional quality assessment of predicted KcsA structures. As the 3D PNP is a semi-quantitative model, thresholds of the functional features should not be too conservative. In this study the following cutoffs were applied:

- Total inward and outward conductance at ±100 mV:

$$G_{in}, G_{out} > 10\ pS,$$

  which is equal to the following condition for the total inward and outward current at ±100 mV:

$$|I_{in}|, |I_{out}| > 1\ pA.$$

  Note that this threshold corresponds to roughly 1/2 of the computational inward conductance and 2/3 of the computational outward conductance of the original KcsA structure 3FB8 [30].

- Inward and outward cation to anion selectivity ratio were arbitrary set to:

$$G^+_{in}/G^-_{in} = I^+_{in}/I^-_{in} > 10:1 \text{ or } 50:1,$$

$$G^+_{out}/G^-_{out} = I^+_{out}/I^-_{out} > 10:1 \text{ or } 50:1$$

- Outward rectification at ±100 mV:

$$G_{out}/G_{in} = |I_{out}/I_{in}| > 1.0.$$

The above defined thresholds provide a intuitive notion of functionally admissible model-structures. In addition we assume that a predicted model is *conducting* when its calculated inward and outward conductance are both within the range of 1 pS and 1 nS. The value of 1 pS is often regarded as the bottom threshold for ionic channels [41]. We also found that the conductance above 1 nS is an indicator of a porous, leaky protein structure (i.e. a structure with multiple erroneously created pores).

2.3 Predictive power of functional characteristics

The functional features were assessed in terms of their ability to select models that are structurally closest to the native protein. For this purpose, functionally correct models were regarded as properly classified only if their general C_α-C_β RMSD (or RMSE of the electrostatic profile) was below a selected threshold. Quality of binary classification at particular threshold was evaluated in terms of Sensitivity (Sn), Specificity (Sp).

$$Sn = \frac{TP}{TP + FN}$$

$$Sp = \frac{TN}{TN + FP}$$

where TP denotes the True Positive rate, which expressed the rate of functionally correct models that were also structurally correct (i.e. below a selected RMSD or RMSE threshold); TN is a True Negative rate with functionally incorrect models that were also structurally incorrect; FP is the False Positive rate with functionally correct models which were structurally incorrect; FN is the False Negative rate with functionally incorrect models that were structurally correct. Additionally, Matthew's correlation coefficient (MCC) and Accuracy (ACC) were also calculated:

$$MCC = \frac{TP \cdot TN - FP \cdot FN}{\sqrt{(TP + FP)(TP + FN)(TN + FP)(TN + FN)}},$$

$$ACC = \frac{TP + TN}{TP + TN + FP + FN}.$$

Overall performance of classification at various thresholds was analyzed using the Area Under Receiver Operating Characteristic curve ($AUROC$) [42].

The TOP100 sets consisted of 100 models which had the lowest deviations (general C_α-C_β RMSD, electrostatic profile RMSE) or the highest plain values (inward selectivity and outward selectivity) of each feature. In case of the RMSD-based ranking, models 98th to 107th had exactly the same quality and were all included in the TOP100. In addition to the simple rankings, two joint rankings (RMSD & RMSE, and inward & outward selectivity) were generated such that both simple rankings were extended to n models until their cross-section counted 100 models.

3 Results and Discussion

3.1 Relation between structural and functional features

Full contact map set

In the first experiment, structures of the KcsA channel were reconstructed based on the full contact map. The total of 430 structural models were generated, 343 of them were *conducting*, i.e. achieved predicted conductance within the range of 1 pS and 1 nS.

All the candidate models were structurally correct as their full atom RMSD to the original PDB structure was between 2 and 2.8 Å. However, in terms of functionality, only 29% of models achieved cation/anion selectivity of 50:1 in both directions, 38% exhibited correct outward rectification, and 77% achieved conductance of 10 pS in both directions. The three functional criteria were fulfilled together by only 37 models, which was roughly 10% of the whole set.

To gain more insight, Kendall's τ coefficients were calculated between structural and functional features. The general full atom RMSD of models correlated significantly with deviation of the inward anionic current ΔI^-_{in} (Tab. S1). Moreover, the deviation of functional features depended on amino acids around selectivity filter, as expected (see Fig. 1A). The strongest association was a positive correlation between rectification $|I_{out}/I_{in}|$ and the pore diameter at THR75, at the intracellular entrance to the selectivity filter (p-value ˜ 1e-10, Fig. 1B). Other highly significant correlations included the RMSD of THR75 and deviation of rectification $\Delta(I_{out}/I_{in})$ and between the RMSD of PRO83 and deviation of the inward anionic current ΔI^-_{in}.

Reduced contact map sets

In the second experiment, protein models were generated from four randomly reduced contact map sets characterized by different information completeness: 90%, 70%, 50% and 30%. Over 4/5 of all models achieved full atom RMSD below 4 Å, including all models rebuilt from maps containing 70% or more contact information (Tab. S2). However, this high RMSD threshold was reached only by 1.4% of models obtained from 30%-complete maps. In addition, the full atom RMSD of 2/5 of all models was below 2.5 Å. Median C_α-C_β RMSD ranged from very good, i.e. 0.76 Å for full contact maps, to poor, i.e. 6 Å for 30%-complete maps (Fig. 2a and Tab. S2). Similar pattern was observed by the full atom RMSD (from 2.39 Å to 6.9 Å,

respectively, Fig. 2a (inset) and Tab. S2).

Functionally, the inward and outward conductance was within the range of 1 pS to 1 nS (*conducting* models) for 1687 (78%) models, and exceeded 10 pS in 72% *conducting* models (Tab. 2). The outward direction of rectification $|I_{out}|/|I_{in}| > 1$ was obtained for 41-51% models, depending on the contact map completeness. The median value of rectification oscillated between 0.9 and 1.0 (Fig. 2d) and typically was significantly below the level of 1.39 calculated for the reference structure. The inward and outward selectivity above 10:1 was reached by only 26% predicted KcsA structures (Tab. 2), a few models reached the inward selectivity level of the original structure (181:1), despite relatively high randomness (Fig. 2c). Selectivity over 50:1 was obtained for just 11% models. Proportion of highly selective models decreased dramatically with reduced information in the map, for example only 2 out of 250 structures from the 30%-complete maps had selectivity higher than 10:1 in comparison to 193 out of 343 structures from the full map. All the functional criteria including the selectivity above 10:1, were collectively fulfilled by 9% of models (almost a half of them were from the full contact maps). Only half of them exhibited selectivity above 50:1. No structure obtained from the 30%-complete maps met all the functional criteria.

General RMSDs (C_α-C_β and full atom) and deviation of charge selectivity were the most and second most correlated pairs of model features, in terms of Kendall's τ (Tab. S3 and Fig. S1). Deviation of the inward current was the third most correlated functional feature (0.21-0.24), while correlation of deviation of the outward current was much weaker (0.12-0.15), yet still statistically significant. Interestingly, correlation of deviation of the rectification with deviation of any structural feature never exceeded range of τ between -0.09 and 0.07.

Discussion.

Significant correlations between structural RMSD, and functional deviations of the charge selectivity and the total current (Tab. S3), support the hypothesis that predicted structural models could be validated on the basis of their calculated functional features related to experimental data. Deviation of the anionic current (experimentally equal to zero) was typically even more highly correlated with structural features than the charge selectivity (τ higher up to 0.40, see Fig. S2), consistently with the result based on the full contact maps (Tab. S1). However, as experimental studies usually do not report the anionic current, further analyzes would focus on the selectivity. Interestingly, a significant difference in selectivity between 90%-complete and 100%-complete map models suggests that this feature can be used to distinguish between good and very good models. The rectification could be, perhaps, more useful for fine tuning of the structure, as suggested by its relatively high correlations with some structural features in the dataset based on the full contact maps

only (Tab. S1). However, it could be also that 3D PNP Solver is least suited to correctly predict rectification (see [30]).

The total current typically increased with decreasing completeness of the map (Fig. 2b). This suggested a tendency of the reconstruction pipeline to produce sparser models (with a larger pore diameter) when information in the contact map was reduced. A larger pore diameter could also explain why the median cation to anion selectivity was of an order weaker for structures built from the 30%-complete maps than from the full maps (Fig. 2c). Indeed, the cation to anion selectivity in the classical electrodiffusion model applied by 3D PNP Solver is a result of presence of negative charges in the selectivity filter and its surroundings, which prevents passage of negatively charged ions. The effect decreases when the selectivity filter diameter is larger than the grid resolution (here: 2 Å), as in such case, the pore is represented by two or more computational cells in the grid and therefore negative charges in the protein wall are partially shielded by positive charges in the solution. Thus, the classical electrodiffusion model performs better when the pore intersection is represented by only one computational cell – in this case the model is consistent with the single-file ion diffusion through the selectivity filter [43, 44].

The six residues, which exhibited the highest structure-function correlations are shown in Fig. 3. GLY79 is situated at the extracellular entrance to the selectivity filter (SF). Therefore, any change in its position or conformation is likely to result in a deviation of the ion flux. ASP80 (not shown, $\tau > 0.30$ only for the oxygen position) takes part in the transformation of SF to the non-conductive conformation [45]. GLY104 is located in another region of the protein important for inactivation kinetics. It is adjacent to PHE103, which has been recently reported to act as an interface between the inner helical bundle and SF [45]. It is possible that the RMSD measure is more sensitive to deviation of atom positions in the small GLY104 than in the large PHE103. Prolines are typically structurally important elements of a protein. Indeed, PRO83 is conserved among several K^+ channels, moreover its position is next to TYR82, another large functionally important residue (see [45] supplementary information). PRO63, while quite away from SF, is adjacent to large ARG64, one of the residues crucial for the inactivation event [46]. A functional role of GLY88 remains unknown, however mutations at this position were linked to disruption of tetramerization [47].

3.2 Predictive power of functional characteristics

Model classification using functional features

In this section, we examine if computed functional characteristics of the ion flux can be used to discriminate between structurally correct and incorrect models. In a systematic analysis, we tested various

thresholds for four functional features: deviations of inward and outward current, and deviations of inward and outward selectivity. The results formed the basis in a search for the optimal discriminative values which would allow for the most reliable model classification in relation to *the ground truth* given by the general C_α-C_β RMSD. Only 1674 *conducting* models were considered. The C_α-C_β RMSD thresholds were fixed at values of 1 Å (highly accurate) and 3 Å (correct). The optimal thresholds were selected according to the maximum product of sensitivity (Sn) and specificity (Sp). Classification quality was evaluated also in terms of accuracy (ACC) and Matthew's correlation coefficient (MCC) at the optimal threshold, and in terms of the area under the ROC curve ($AUROC$) as a summary measure over all thresholds (Tab.3).

The classification based on deviation of the inward selectivity produced ROC curves which were well above the diagonal for both RMSD thresholds ($AUROC$ $0.72-0.78$) and shifted towards specificity (Fig. 4). The classification based on the current deviation resulted in similar $AUROC$ for the RMSD of 3 Å, while it was lower for the 2 Å threshold ($AUROC$ $0.59-0.65$). In this cases the ROC curve was shifted towards sensitivity. The deviation of selectivity displayed the best balance between retaining good quality models and rejecting structurally incorrect models (MCC $0.38-0.39$). Overall performance of the classification was better for higher RMSD thresholds. The optimal thresholds were relatively lower for the outward direction of selectivity (by 14-18%), and for the inward direction of current (by 8-20%). In practical terms, applying the optimal thresholds of selectivity retained ca. 70% of structurally correct models (518-548 out of 752 models with RMSD < 1 Å, and 940-1015 out of 1412 models with RMSD < 3 Å) at the cost of retaining 15-33% of structurally incorrect models in the group of functionally correct models (288-313 out of 935 models with RMSD ≥ 1 Å, and 42-69 out of 275 models with RMSD ≥ 3 Å). Using the optimal thresholds of current deviations as a classifier resulted in retaining 71-82% of correct models and 41-66% of incorrect models.

Electrostatic RMSE as a complementary ground truth

In section , we reported that a significant proportion of models were non-*conducting* while having a relatively low general RMSD. This raised doubts whether general RMSD was an appropriate solitary measure of the channel structure quality. Therefore, we propose the electrostatic potential profile in the native channel structure as a new *ground truth* (Fig. 5a), and its Root Mean Square Error (RMSE) as an alternative to the entirely structure-based RMSD. It can be argued that the RMSE of the electrostatic potential profile is a measure that balances the structural and functional quality of the channel model as the electrostatic potential profile is determined by the structure, and determines the channel function at the same time. While the electrostatic potential profile cannot be measured experimentally, it could be used to assess the relationship between structural and functional quality, and to evaluate the predictive power of calculated

current-voltage characteristics.

First, we established the relation between the structural RMSD and the electrostatic RMSE threshold (Fig. 5b). We found that the electrostatic profile RMSE and the general C_α-C_β RMSD were generally well correlated. (Kendall's $\tau = 0.45$). However, the relation was much weaker for low RMSD structures ($\tau = 0.12$ for RMSD < 1.7 Å). In this group consisting of the most accurate models the two characteristics were complementary to each other.

Next, we searched for the optimal thresholds for the four functional features (the inward and outward, current and selectivity deviations) to obtain the most reliable classification in terms of specificity and sensitivity product, related to the electrostatic RMSE at fixed thresholds of 0.3, 0.4 and 0.5 V. Again, only the *conducting* models were considered. Generally, classification characteristics were similar as in the case of classification in relation to the structural RMSD (Fig. 6 and Tab. S4). Interestingly, overall performance of the classification was more sensitive to changing the threshold of *the ground truth* than in the RMSD-related experiment. This finding is consistent with presumably closer relationship between the current-voltage characteristics and the electrostatic profile.

Practical scenarios

In this section, two practical scenarios of our model quality assessment approach are analyzed. In order to emulate the-real-life use cases plain values of functional features were used instead of deviations related to the true structure.

In the first scenario, the goal was to reduce a collection of candidate structural models. They were subjected to criteria of functional correctness in reference to available experimental current-voltage characteristics. The criteria were rather liberal, keeping in mind the semi-quantitative character of the 3D PNP model. We checked how applying intuitive functional conditions (defined in Sec 2.2) reduces the dataset and enriches it in structures with low general C_α-C_βRMSD and profile RMSE (Tab. 4 top).

None of conductance conditions improved quality of the resulting subset in comparison to the initial dataset (Fig. 7a). Unlike that, enrichment in high quality candidates due to the selectivity criteria was substantial (Fig. 7b). Virtually all structures with selectivity ratio above 10:1 were within RMSD<3 Å and RMSE<0.5 V from the real structure in comparison to ca. 80% in the whole population. Moreover, fraction of highly accurate structures increased from 44% to 75% (RMSD<1 Å) or from 38% to 57% (RMSE<0.3 V). The improvement was even more pronounced with the more stringent selectivity criteria (increase of highly accurate fraction by almost 90%). Median RMSD and RMSE were reduced by 20-30% and all exceptionally

wrong models were filtered out (no RMSD/RMSE was above 5.44 Å/0.58 V for S10 or above 2.61 Å/0.45 V for S50, Fig. 7a). Finally, adding the outward rectification condition slightly worsened the candidate set in terms of enrichment in structurally and electrostatically accurate models (Fig. 7a).

In the second scenario, the goal was to select the best 100 candidate models (TOP100). We checked to what extent the 100 best models in terms of the cation to anion selectivity overlap with the 100 best models in terms of the general C_α-C_β RMSD and/or the profile RMSE (see Tab. 4 bottom). Models were ranked separately in four simple categories: general C_α-C_β RMSD, profile RMSE, inward selectivity, outward selectivity, and in two joint categories: RMSD & RMSE and inward & outward selectivity (See Methods). In TOP100[RMSD] the RMSD ranged from 0.717 to 0.749 Å, in TOP100[RMSE] the RMSE ranged from 0.098 to 0.171 V, and in TOP100[RMSD&RMSE] the RMSD ranged from 0.717 to 0.774 Å and the RMSE ranged from 0.121 to 0.232 V. In TOP100 $[\frac{I^+_{in}}{I^-_{in}}]$ the inward selectivity ranged from 70:1 to 192:1, , in TOP100$[\frac{I^+_{out}}{I^-_{out}}]$ the outward selectivity ranged from 108:1 to 518:1, and in TOP100$[\frac{I^+_{in}}{I^-_{in}}\&\frac{I^+_{out}}{I^-_{out}}]$ the inward selectivity ranged from 62:1 to 185:1 and the outward selectivity ranged from 89:1 to 518:1.

Probability of finding a TOP100 model from the *ground-truth*-based ranking by chance was less than 5%. The odds increased drastically when only the 100 most cation selective models were considered. Most notably, the TOP100 according to outward selectivity included 33 out of the best 100 models in terms of the joint RMSD and RMSE criterion (7 times better than random). Enrichment in the TOP100 based on the inward selectivity was weaker but still significant (from 1.9 times for TOP100[RMSD] to 4.1 times for TOP100[RMSD&RMSE]). Enrichment in the TOP100 based on the joint ranking of inward and outward selectivity ranged from 2.6 to 4.8 times, depending on the *ground truth*.

Discussion

Fairly good *AUROC* values for classification based on the selectivity and current deviations showed that the features are sensitive to structural and electrostatic quality of models and therefore are suitable for separating models with low and high structural RMSD or electrostatic profile RMSE. However, ranges of current defined by the optimal deviation thresholds were below experimental values of the current (Tab. 1 and Tab. 3). In addition, we found that liberal thresholds of current, taking into account approximate accuracy of the classical 3D PNP model, could not be effectively used to filter out structurally or electrostatically inaccurate models. Consequently, with the classical electrodiffusion model, the current-based criterion can be employed only for eliminating models with an occluded pore or with multiple erroneously created pores.

The optimal thresholds for selectivity deviation translate to selectivity cutoff ranging from 2.3:1 (inward selectivity, RMSD<3 Å) to from 4.1:1 (outward selectivity, RMSD<1 Å). These cutoff were severely underestimated in reference to experimental data (no anionic current) and to computational results for the original structure (Tab. 1). However, due to very good specificity of the selectivity-based classification (i.e. retrieving ca. 20% of structurally accurate models with a few false positives, Fig. 4cd), the condition of high selectivity (above 10:1) proved to be practical for model quality assessment (Tab. 4 and Fig. 7). While it requires further studies to verify if the semi-quantitative accuracy of the classical 3D PNP in predicting selectivity is sufficient for assessment of candidate models of mildly-selective channels (such as alpha-hemolysin, GLIC, etc.), the present study showed that the method is appropriate for the class of strongly-selective channels.

4 Conclusions

In this study, we proposed a novel function-oriented approach to the single model quality assessment which is complementary to existing methods. The approach is applicable to analysis of structural models of proteins whose quantitative functional characteristics are known. This general idea was applied to quality assessment of structural models of potassium channel KcsA generated from contact maps of varying quality. The evaluation was based on current-voltage characteristics computed for predicted structures using the classical 3D Poisson-Nernst-Planck model, which were compared to available results from patch-clamp experiments.

We found that structural quality of candidate models, in terms of RMSD to the original structure, was significantly correlated with predicted conductance and charge selectivity (Kendall's rank correlation up to 0.4). This supported the initial hypothesis that predicted structural models could be validated on the basis of their calculated functional features related to experimental data. It was further confirmed by good performance in separating models with low and high RMSD on the basis on deviation of current and selectivity from their values computed for the true structure ($AUROC$ up to 0.78).

In practical terms, our approach had to deal with limitations of the classical 3D PNP, which is a fast but approximate method and could not accurately reproduce experimental characteristics for the reference structure. Therefore, cutoff thresholds for assessing functional correctness of a model had to be set liberally. Under these conditions, we showed that evaluating predicted conductance was an appropriate method to eliminate modes with an occluded pore or with multiple erroneously created pores. In addition, filtering models on the basis of their predicted charge selectivity resulted in a substantial enrichment of the candidate set in highly accurate models. E.g. by demanding the charging selectivity above 10:1, we obtained a high accuracy subset containing 21% candidate models of which 99% had C_α-C_β RMSD below 3 Å. This shows that the method can be directly applied for evaluation of structural models of at least strongly-selective

protein channels. Moreover, it can be expected that efficiency of our model quality assessment method will improve when more accurate and comparably fast continuous models of ion flow in a protein channel are available.

Our work raises an important question how to define correctness of an ion channel model. Is the general RMSD an appropriate *ground truth* measure in this context? We found that a significant proportion of models were occluded while having a low general RMSD. It is unlikely that this could be uniquely attributed to the coarse resolution and discretization used in the PNP calculations. In addition, an important variation of electrostatic profiles was found in a group of models characterized by C_α-C_β RMSD below 1 Å. Therefore, we investigated using the electrostatic potential profile of the reference structure as a complementary *ground truth*. Not surprisingly, models with low and high RMSE of the electrostatic profile were well separated on the basis of deviation of current and selectivity ($AUROC$ up to 0.76). Very interestingly, the selection of 100 best models in terms of the selectivity was significantly more enriched in TOP100 models with the the joint lowest RMSE and RMSD than in models with the lowest RMSD. While the electrostatic profile cannot be measured experimentally, our results indicate that predicted current-voltage characteristics convey information about electrostatics. This important information about correctness of a model is complementary to the general RMSD. This suggests that, perhaps, the computational validation of functionality should be included in the evaluation process of structural models whenever possible.

Acknowledgments

This research was partially supported by National Science Center grant no N N519 643540 for M.Kotulska, scholarship START of Foundation for Polish Science for W.Dyrka and from the budget for science in 2012-2015 as a research project within the program "Diamond Grant" DI2011 002141 for M.Kurczynska. Some of the calculations have been performed in Wroclaw Center for Networking and Supercomputing.

References

[1] H. M. Berman, J. Westbrook, Z. Feng, G. Gilliland, T. T. Bhat, H. Weissig, I. N. Shindyalov, P. E. Bourne, The Protein Data Bank, Nucleic Acid Research 28 (2000) 235–242.

[2] A. Winter, A. P. Higueruelo, M. Marsh, A. Sigurdardottir, W. R. Pitt, T. L. Blundell, Biophysical and computational fragment-based approaches to targeting protein-protein interactions: applications

in structure-guided drug discovery, Quarterly Reviews of Biophysics 45 (2012) 383–426. doi:10.1017/S0033583512000108.

[3] G.-F. Hao, G.-F. Yang, C.-G. Zhan, Structure-based methods for predicting target mutation-induced drug resistance and rational drug design to overcome the problem, Drug Discovery Today 17 (19-20) (2012) 1121 – 1126. doi:http://dx.doi.org/10.1016/j.drudis.2012.06.018.

[4] Z. Lou, X. Zhang, Protein targets for structure-based anti-mycobacterium tuberculosis drug discovery, Protein & Cell 1 (5) (2010) 435–442. doi:10.1007/s13238-010-0057-3.

[5] N. Koga, R. Tatsumi-Koga, G. Liu, R. Xiao, T. B. Acton, G. T. Montelione, D. Baker, Principles for designing ideal protein structures, Nature 491 (2012) 222–227.

[6] J. Moult, K. Fidelis, A. Kryshtafovych, T. Schwede, A. Tramontano, Critical assessment of methods of protein structure prediction (casp) - round x, Proteins: Structure, Function, and Bioinformatics 82 (2014) 1–6.

[7] A. Zemla, C. Venclovas, J. Moult, K. Fidelis, Processing and analysis of casp3 protein structure predictions, Proteins ;Suppl 3 (1999) 22–29.

[8] L. Rychlewski, D. Fischer, A. Elofsson, Livebench-6: large-scale automated evaluation of protein structure prediction servers, Proteins; Suppl 536 (2003) 542–547.

[9] A. R. Ortiz, C. E. Strauss, O. Olmea, Mammoth (matching molecular models obtained from theory): an automated method for model comparison, Protein Sci 11 (11) (2002) 2606–2621.

[10] M. R. Betancourt, J. Skolnick, Universal similarity measure forcomparing protein structures, Biopolymers 59 (5) (2001) 305–309.

[11] L. Holm, C. Sander, Dali: a network tool for protein structure comparison, Trends Biochem Sci 20 (11) (1995) 478–480.

[12] B. A. Reva, A. V. Finkelstein, J. Skolnick, What is the probability of a chance prediction of a protein structure with an rmsd of 6 a, Fold Des 3 (2) (1998) 141–147.

[13] Y. Zhang, J. Skolnick, Scoring function for automated assessment of protein structure template quality, Proteins 57 (4) (2004) 702–710.

[14] J. Cheng, Z. Wang, A. N. Tegge, E. J, Prediction of global and local quality of casp8 models by multicom series, Proteins 77 (2009) 181–4.

[15] Q. Wang, K. Vantasin, D. Xu, Y. Shang, Mufold-wqa: A new selective consensus method for quality assessment in protein structure prediction, Proteins 79 (2011) 185–95.

[16] M. Skwark, A. Elofsson, Pconsd: ultra rapid, accurate model quality assessment for protein structure prediction, Bioinformatics 29 (2013) 1817–8.

[17] B. M. Konopka, J.-C. Nebel, M. Kotulska, Quality assessment of protein model-structures based on structural and functional similarities, BMC Bioinformatics 13 (2012) 242.

[18] L. J. McGuffin, M. T. Buenavista, D. B. Roche, The modfold4 server for the quality assessment of 3d protein models, Nucleic Acids Res. 41 (2013) W368–72.

[19] B. Wallner, A. Elofsson, Identification of correct regions in protein models using structural, alignment, and consensus information, Protein Sci. 15 (2006) 900–13.

[20] P. Benkert, S. C. Tosatto, D. Schomburg, Qmean: A comprehensive scoring function for model quality assessment, Proteins 71 (2008) 261–77.

[21] A. Ray, E. Lindahl, B. Wallner, Improved model quality assessment using proq2., BMC Bioinformatics 13 (2012) 224.

[22] O. Hamill, A. Marty, E. Neher, B. Sakmann, F. Sigworth, Improved patch-clamp techniques for high-resolution current recording from cells and cell-free membrane patches, Pflugers Arch 391 (1981) 85–100.

[23] H. S. Randa, L. R. Forrest, G. A. Voth, M. S. Sansom, Molecular dynamics of synthetic leucine-serine ion channels in a phospholipid membrane, Biophysical Journal 77 (5) (1999) 2400 – 2410.

[24] W. Im, B. Roux, Ions and counterions in a biological channel: A molecular dynamics simulation of OmpF porin from escherichia coli in an explicit membrane with 1 M KCl aqueous salt solution, Journal of Molecular Biology 319 (5) (2002) 1177 – 1197.

[25] S.-H. Chung, T. W. Allen, M. Hoyles, S. Kuyucak, Permeation of ions across the potassium channel: Brownian dynamics studies, Biophysical Journal 77 (5) (1999) 2517 – 2533.

[26] D. Marreiro, M. Saraniti, S. Aboud, Brownian dynamics simulation of charge transport in ion channels, Journal of Physics: Condensed Matter 19 (21) (2007) 215203.

[27] M. G. Kurnikova, R. D. Coalson, P. Graf, A. Nitzan, A lattice relaxation algorithm for three-dimensional Poisson–Nernst–Planck theory with application to ion transport through the gramicidin A channel, Biophysical Journal 76 (1999) 642–656.

[28] S. Y. Noskov, W. Im, B. Roux, Ion permeation through the a-hemolysin channel: Theoretical studies based on brownian dynamics and Poisson–Nernst–Plank electrodiffusion theory, Biophysical Journal 87 (2004) 2299–2309.

[29] W. Dyrka, A. T. Augousti, M. Kotulska, Ion flux through membrane channels - an enhanced algorithm for the Poisson–Nernst–Planck model, Journal of Computational Chemistry 29 (12) (2008) 1876–1888.

[30] W. Dyrka, M. Bartuzel, K. M, Optimization of 3d poisson-nernst-planck model for fast evaluation of diverse protein channels, Proteins 81 (2013) 1802–1822, under revision.

[31] S. Furini, C. Domene, M. Rossi, M. Tartagni, S. Cavalcanti, Model-based prediction of the alpha-hemolysin structure in the hexameric state, Biophysical journal 95 (5) (2008) 2265–2274.

[32] M. LeMasurier, L. Heginbotham, C. Miller, KcsA, The Journal of General Physiology 118 (3) (2001) 303–314.

[33] B. M. Konopka, M. Ciombor, M. Kurczynska, M. Kotulska, Automated procedure for contact-map-based protein structure reconstruction, J. Membr. Biol. 247 (2014) 409–20.

[34] J. Duarte, R. Sathyapriya, H. Stehr, I. Filippis, M. Lappe, Optimal contact definition for reconstruction of contact maps, BMC Bioinformatics 11 (1) (2010) 283.

[35] M. Vassura, L. Margara, P. D. Lena, F. Medri, P. Fariselli, R. Casadio, Reconstruction of 3d structures from protein contact maps, IEEE/ACM Transactions on Computational Biology and Bioinformatics 5 (3) (2008) 357–367.

[36] M. Vassura, L. Margara, P. D. Lena, F. Medri, P. Fariselli, R. Casadio, Ft-comar: fault tolerant three-dimensional structure reconstruction from protein contact maps, Bioinformatics 24 (10) (2008) 1313–1315.

[37] J. Maupetit, R. Gautier, P. Tuffery, Sabbac: online structural alphabet-based protein backbone reconstruction from alpha-carbon trace, Nucleic Acids Research 34 (2006) W147–W151.

[38] G. G. Krivov, M. V. Shapovalov, R. L. Dunbrack Jr., Improved prediction of protein side-chain conformations with scwrl4, Proteins 77 (2009) 778–795.

[39] N. A. Baker, D. Sept, S. Joseph, M. J. Holst, J. A. McCammon, Electrostatics of nanosystems: Application to microtubules and the ribosome, Proceedings of the National Academy of Sciences 98 (18) (2001) 10037–10041.

[40] M. Kendall, A new measure of rank correlation, Biometrika 30 (1938) 81–89.

[41] H. Jayaram, A. Accardi, F. Wu, C. Williams, C. Miller, Ion permeation through a Cl--selective channel designed from a CLC Cl-/H+ exchanger, Proceedings of the National Academy of Sciences 105 (32) (2008) 11194–11199.

[42] T. Fawcett, An introduction to roc analysis, Pattern Recognition Letters 27 (8) (2006) 861–874.

[43] A. L. Hodgkin, R. D. Keynes, The potassium permeability of a giant nerve fiber, J. Physiol. (Lond.) 128 (1955) 61.

[44] H.-H. Kohler, A single-file model for potassium transport in squid giant axon simulation of potassium currents at normal ionic concentrations, Biophys. J. 19 (2) (1977) 125–140.

[45] L. G. Cuello, V. Jogini, D. M. Cortes, E. Perozo, Structural mechanism of C-type inactivation in K+ channels, Nature 466 (7303) (2010) 203–208.

[46] J. F. Cordero-Morales, L. G. Cuello, Y. Zhao, V. Jogini, D. M. Cortes, B. Roux, E. Perozo, Molecular determinants of gating at the potassium-channel selectivity filter, Nature Structural & Molecular Biology 13 (2006) 311 – 318.

[47] S. N. Irizarry, E. Kutluay, G. Drews, S. J. Hart, L. Heginbotham, Opening the KcsA K+ channel: Tryptophan scanning and complementation analysis lead to mutants with altered gating, Biochemistry 41 (46) (2002) 13653–13662.

Figures captions

Figure 1: Kendall's rank correlations of amino acid RMSD and deviations of functional features in models reconstructed from full contact maps. **(A)** All significant correlations (p-value$\leq$0.01) between an amino acid RMSD and deviations of at least 2 (blue) or 1 (cyan) functional features. **(B)** The strongest correlation was observed between the pore diameter at THR75 (orange) and rectification. Other strong correlations included the RMSD of THR75 and deviation of rectification; and the RMSD of PRO83 (pink) and deviation of the inward anionic current.

Figure 2: Structural and functional quality of reconstructed KcsA models. **(a)** Structural Cα-Cβ (**main**) and full atom (**inset**) RMSD of predicted KcsA structures in subsets built using various percentages of contact maps. **(b-d)** Functional characteristics of predicted KcsA structures in 100mM KCl at $\pm$100 mV, only the *conducting* models were considered. **(b)** total outward and inward currents, **(c)** outward and inward cation to anion selectivity, and **(d)** rectification (outward to inward current ratio). Notations: whiskers - min and max, box edges - 25% and 75% percentile, inner line - median, dotted line indicates value calculated for the reference structure.

Figure 3: Most significant Kendall's rank correlations of amino acid RMSD and deviations of functional features in all models. Notations: black - LEU40, gray - PRO63 (outside of the protein) and PRO83 (middle of the protein), white - GLY79 (extracellular entrance to the SF), GLY88 (outside of the channel) and GLY104 (intracellular entrance to the channel)

Figure 4: ROC curves of model classification based on deviations of current and selectivity at four thresholds of the general C_α-C_β RMSD. Only the *conducting* models were considered. The RMSD thresholds corresponded to the following positive/negative ratios: 1 Å: 752/935, 2 Å: 1229/458, 3 Å: 1412/275, 4 Å: 1499/188.

Figure 5: Electrostatic profile RMSE as a complementary *ground truth*. **(a)** Exemplary electrostatic profiles of the reference channel pore (solid) and two modeled channel pores: correct (dashed line) and incorrect (dash-dotted line). **(b)** Scatter plot of the electrostatic profile RMSE versus the general C_α-C_β RMSD. The axes have been cut at the 10 Å and 1 V thresholds of RMSD and RMSE, respectively. Both measures are overall well correlated (Kendall's $\tau = 0.45$), the relation is much weaker for low RMSD structures ($\tau = 0.12$ for RMSD < 1.7 Å).

Figure 6: ROC curves of model classification based on deviations of current and selectivity

at three threshold of the electrostatic profile RMSE. Only the *conducting* models were considered. The RMSE thresholds corresponded to the following positive/negative ratios: 0.3 V: 625/1049, 0.4 V: 1025/649, 0.5 V: 1324/350. The AUROC was in the following ranges: (a) 0.61-0.72, (b) 0.56-0.66, (c) 0.64-0.74, (d) 0.66-0.76.

Figure 7: Quality enrichment of the candidate subsets using several functional criteria. **(a)** Box plots of the structural C_α-C_β RSMD and the electrostatic profile RMSE in groups of models fulfilling functional conditions: *cond*: *the conducting models* or 1 pS$<G<$1 nS, C10: $G>$10 pS, S10: $G^+/G^- > 10:1$, S50: $G^+/G^- > 50:1$, RO: $G_{out}/G_{in} > 1$. Notations: red line - median, box edges - 25^{th} and 75^{th} percentile, whiskers - min and max. **(b)** Scatter plot of the electrostatic profile RMSE versus the general C_α-C_β RMSD. The axes have been cut at the 10 Å and 1 V thresholds of RMSD and RMSE, respectively. Color code: green - the *conducting* models with inward and outward selectivities $G^+/G^- > 10:1$, blue - remaining *conducting* models (1 pS$<G<$1 nS), black - all other models.

Tables

Parameter	Experimental	Computational
Inward (-100 mV)		
Total conductance I_{in}	57 pS	15 pS
Cation/anion selectivity I_{in}^{+}/I_{in}^{-}	∞:1	181:1
Outward (+100 mV)		
Total conductance I_{out}	75 pS	21 pS
Cation/anion selectivity I_{in}^{+}/I_{in}^{-}	∞:1	111:1
Rectification $\lvert I_{out}/I_{in}\rvert$	1.29	1.39

Table 1: **Selected experimental [32] and computational [30] parameters of KcsA I-V curves.** Computational results obtained using 3D PNP Solver on the 3FB8 structure.

CMAP	Conducting models	Conductance	Rectification	Selectivity		All criteria incl.	
		$G > 10\,\mathrm{pS}$	$\lvert I_{out}\rvert > \lvert I_{in}\rvert$	$\frac{I^+}{I^-} > 10$	$\frac{I^+}{I^-} > 50$	$\frac{I^+}{I^-} > 10$	$\frac{I^+}{I^-} > 50$
100%	343	265 (77%)	140 (41%)	193 (56%)	101 (29%)	67 (20%)	38 (11%)
90%	354	229 (65%)	182 (51%)	120 (34%)	50 (14%)	43 (12%)	18 (5%)
70%	361	245 (68%)	174 (48%)	98 (27%)	24 (7%)	32 (9%)	10 (3%)
50%	379	277 (73%)	165 (43%)	49 (13%)	19 (5%)	12 (3%)	5 (1.3%)
30%	250	203 (81%)	117 (47%)	2 (.6%)	-	-	-
TOTAL	1687	1219 (72%)	778 (46%)	462 (26%)	194 (11%)	154 (9%)	71 (4%)

Table 2: **Functional quality assessment of models based on randomly reduced contact maps.** The table accounts only for *conducting* models ($1\,\mathrm{pS}<G<1\,\mathrm{nS}$). The CMAP column indicates completeness of randomly reduced contact maps.

Condition	RMSD C_α-C_β	$Sp \cdot Sn$	Sp	Sn	ACC	MCC	$AUROC$
$\Delta I_{in} < 0.80\,\text{pA}$	< 1 Å	0.37	0.52	0.71	0.60	0.23	0.65
$\Delta I_{in} < 1.15\,\text{pA}$	< 3 Å	0.48	0.59	0.82	0.78	0.34	0.75
$\Delta I_{out} < 1.00\,\text{pA}$	< 1 Å	0.32	0.44	0.71	0.56	0.16	0.59
$\Delta I_{out} < 1.25\,\text{pA}$	< 3 Å	0.44	0.55	0.80	0.76	0.29	0.70
$\Delta \frac{I^+_{in}}{I^-_{in}} < 3.90$	< 1 Å	0.48	0.69	0.69	0.69	0.38	0.72
$\Delta \frac{I^+_{in}}{I^-_{in}} < 4.40$	< 3 Å	0.54	0.75	0.72	0.72	0.36	0.76
$\Delta \frac{I^+_{out}}{I^-_{out}} < 3.35$	< 1 Å	0.48	0.67	0.73	0.69	0.39	0.74
$\Delta \frac{I^+_{out}}{I^-_{out}} < 3.60$	< 3 Å	0.56	0.85	0.67	0.70	0.38	0.78

Table 3: **Optimal classification based on selectivity deviation and current deviation related to C_α-C_β RMSD as the *ground truth*.**Only the *conducting* models are considered. The RMSD thresholds corresponded to the following Positive/Negative ratios: 1 Å: 752/935, 3 Å: 1412/275.

Table 4: **Quality enrichment of the candidate subsets using several functional criteria.** Enrichment denotes a fraction of models fulfilling a functional condition which are within a given structural or electrostatic threshold. Functional parameters were calculated only for the *conducting* models. **(top)** The functional conditions were defined as follows: *cond*: the *conducting* models or 1 pS<G<1 nS, C10: G>10 pS, S10: $G^+/G^- > 10:1$, S50: $G^+/G^- > 50:1$, RO: $G_{out}/G_{in} > 1$. **(bottom)** TOP100 denotes the best 100 models fulfilling all conditions given as an argument. Here, the enrichment is effectively a fraction of models which belong to the cross-section of a pair of TOP100 rankings. Note that models 98th to 107th in the C_α-C_β RMSD-based ranking had exactly the same quality (0.749 Å).

Condition	#models	median RMSD	median RMSE	Enrichment [%]			
				RMSD < 1 Å	RMSD < 3 Å	RMSE < 0.3 V	RMSE < 0.5 V
none	2158	1.14	0.35	44	82	38	79
cond	1674	1.12	0.35	45	84	37	79
C10	1213	1.15	0.34	44	82	38	78
S10	458	0.80	0.28	75	99	57	98
S50	191	0.78	0.26	82	100	72	100
S10 & RO	203	0.84	0.32	75	100	41	98
S50 & RO	71	0.78	0.29	75	100	61	100
				TOP100 [RMSD]	TOP100 [RMSE]	TOP100 [RMSD&RMSE]	
none	2158	1.14	0.35	5.0	4.6	4.6	
TOP100[$\frac{I^+_{in}}{I^-_{in}}$&$\frac{I^+_{out}}{I^-_{out}}$]	100	0.78	0.25	13	16	22	
TOP100[$\frac{I^+_{in}}{I^-_{in}}$]	100	0.79	0.26	9.4	16	19	
TOP100[$\frac{I^+_{out}}{I^-_{out}}$]	100	0.78	0.24	18	19	33	

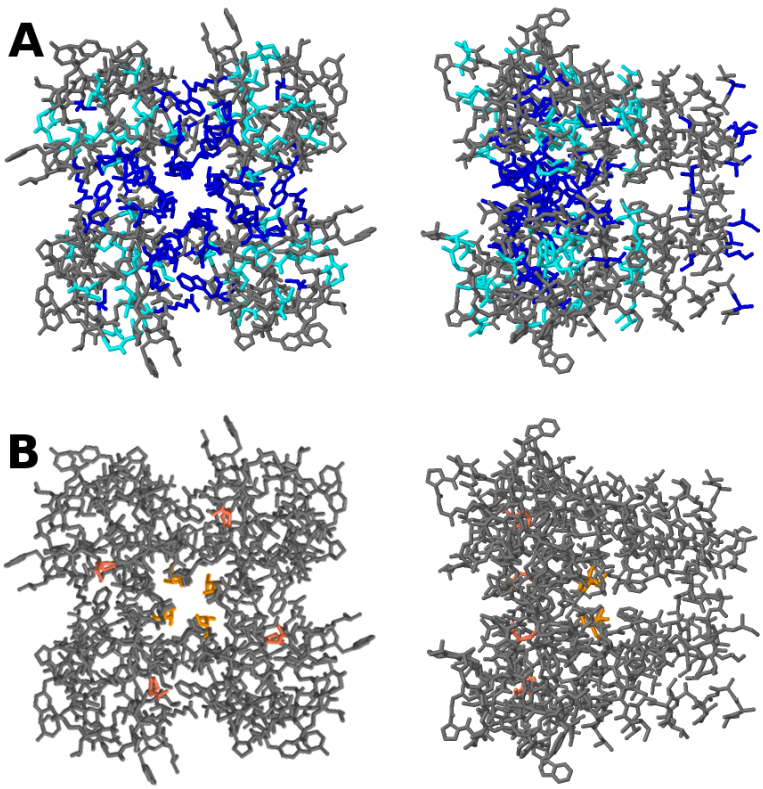

Figure 1: Kendall's rank correlations of amino acid RMSD and deviations of functional features in models reconstructed from full contact maps. **(A)** All significant correlations (p-value$\leq$0.01) between an aminacid RMSD and deviations of at least 2 (blue) or 1 (cyan) functional features. **(B)** The strongest correlation was observed between the pore diameter at THR75 (orange) and rectification. Other strong correlations included the RMSD of THR75 and deviation of rectification; and the RMSD of PRO83 (pink) and deviation of the inward anionic current.

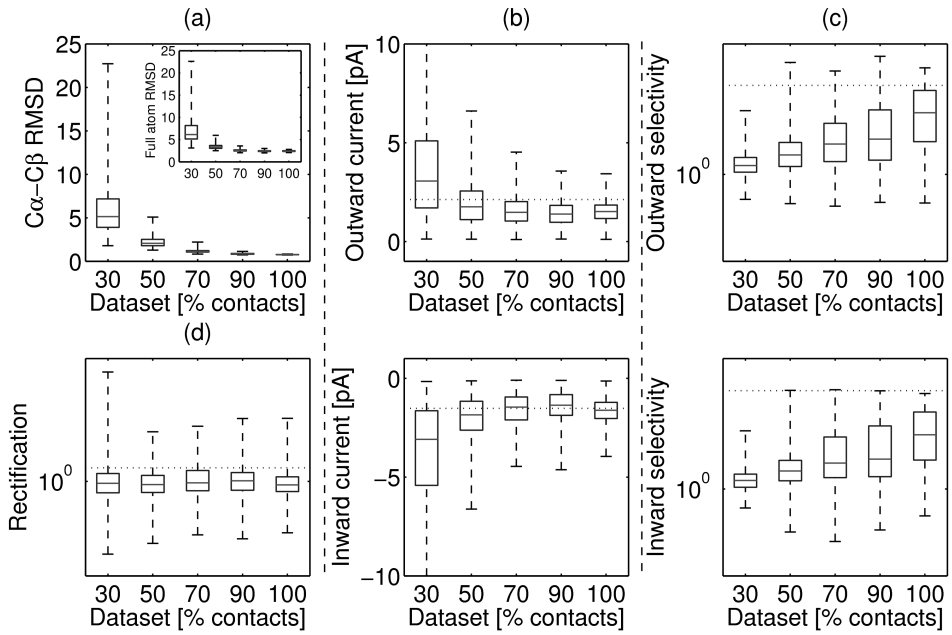

Figure 2: Structural and functional quality of reconstructed KcsA models. **(a)** Structural Cα-Cβ (**main**) and full atom (**inset**) RMSD of predicted KcsA structures in subsets built using various percentages of contact maps. **(b-d)** Functional characteristics of predicted KcsA structures in 100mM KCl at $\pm$100 mV, only the *conducting* models were considered. **(b)** total outward and inward currents, **(c)** outward and inward cation to anion selectivity, and **(d)** rectification (outward to inward current ratio). Notations: whiskers - min and max, box edges - 25% and 75% percentile, inner line - median, dotted line indicates value calculated for the reference structure.

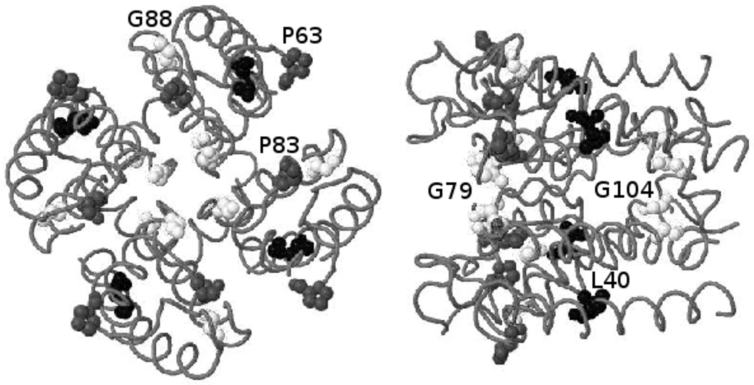

Figure 3: Most significant Kendall's rank correlations of amino acid RMSD and deviations of functional features in all models. Notations: black - LEU40, gray - PRO63 (outside of the protein) and PRO83 (middle of the protein), white - GLY79 (extracellular entrance to the SF), GLY88 (outside of the channel) and GLY104 (intracellular entrance to the channel)

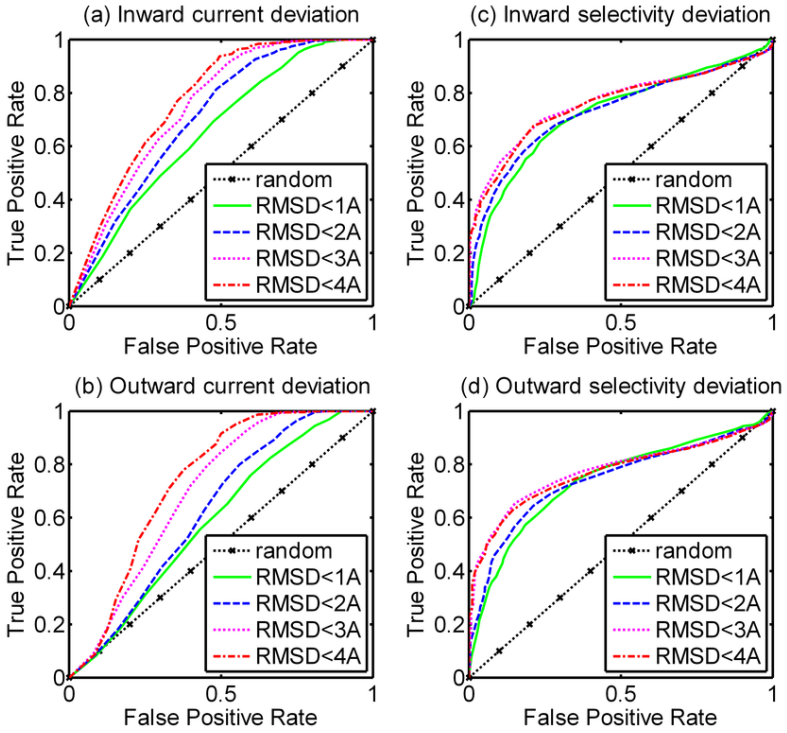

Figure 4: ROC curves of model classification based on deviations of current and selectivity at four thresholds of the general C_α-C_β RMSD. Only the *conducting* models were considered. The RMSD thresholds corresponded to the following positive/negative ratios: 1 Å: 752/935, 2 Å: 1229/458, 3 Å: 1412/275, 4 Å: 1499/188.

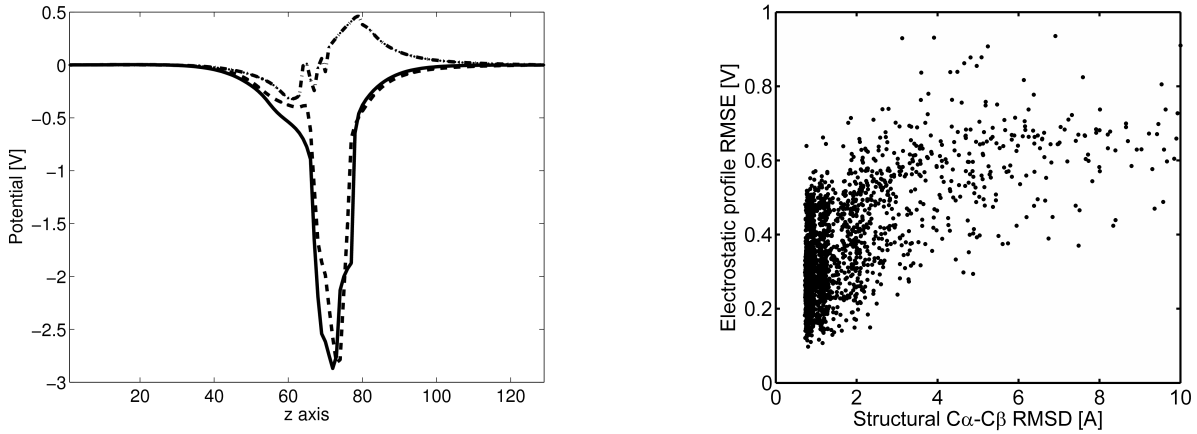

(a) (b)

Figure 5: Electrostatic profile RMSE as a complementary *ground truth*. **(a)** Exemplary electrostatic profiles of the reference channel pore (solid) and two modeled channel pores: correct (dashed line) and incorrect (dash-dotted line). **(b)** Scatter plot of the electrostatic profile RMSE versus the general C_α-C_β RMSD. The axes have been cut at the 10 Å and 1 V thresholds of RMSD and RMSE, respectively. Both measures are overally well correlated (Kendall's $\tau = 0.45$), the relation is much weaker for low RMSD structures ($\tau = 0.12$ for RMSD < 1.7 Å).

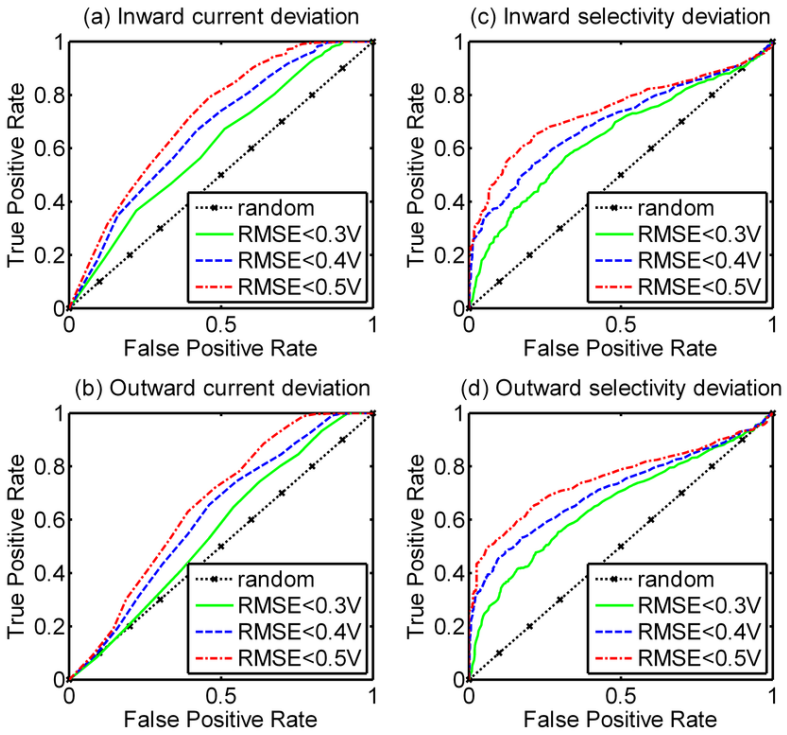

Figure 6: ROC curves of model classification based on deviations of current and selectivity at three threshold of the electrostatic profile RMSE. Only the *conducting* models were considered. The RMSE thresholds corresponded to the following positive/negative ratios: 0.3 V: 625/1049, 0.4 V: 1025/649, 0.5 V: 1324/350. The AUROC was in the following ranges: (a) 0.61-0.72, (b) 0.56-0.66, (c) 0.64-0.74, (d) 0.66-0.76.

Figure 7: Quality enrichment of the candidate subsets using several functional criteria. **(a)** Boxplots of the structural C_α-C_β RSMD and the electrostatic profile RMSE in groups of models fulfilling functional conditions: *cond*: *the conducting models* or 1 pS<G<1 nS, C10: G>10 pS, S10: $G^+/G^- > 10:1$, S50: $G^+/G^- > 50:1$, RO: $G_{out}/G_{in} > 1$. Notations: whiskers - min and max, box edges - 25% and 75% percentile, inner line - median. **(b)** Scatter plot of the electrostatic profile RMSE versus the general C_α-C_β RMSD. The axes have been cut at the 10 Å and 1 V thresholds of RMSD and RMSE, respectively. Notations: magenta - the *conducting* models with inward and outward selectivities $G^+/G^- > 10:1$, black - all other models.

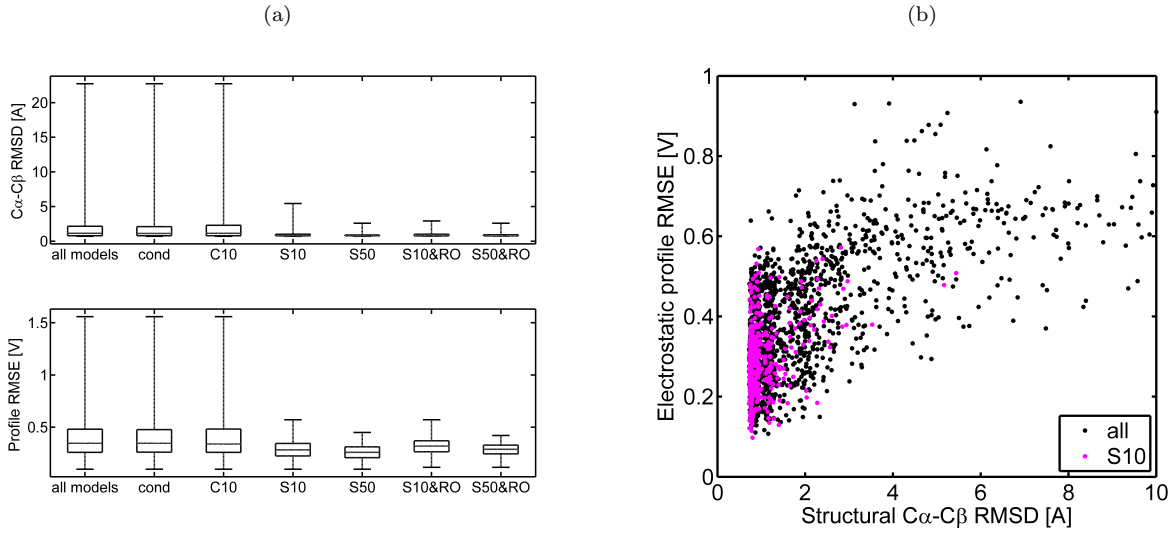

Supplemental Data

Supplemental Table 1

Structural feature	Functional feature	τ	p-value
Pore diameter at THR75	$\lvert I_{out}/I_{in}\rvert$	0.23 - 0.24	2.4×10^{-10} – 5.5×10^{-11}
RMSD of THR75	$\Delta(I_{out}/I_{in})$	0.14 - 0.21	6.5×10^{-5} – 2.9×10^{-9}
RMSD of PRO83	ΔI_{in}^-	0.20	2.3×10^{-8}
General full atom RMSD	ΔI_{in}^-	0.19	1.9×10^{-7}

Most significant Kendall correlations between structural and functional features based on the full contact map set. Note that side chains of reconstructed tetramers of KcsA were not perfectly symmetric which in case of THR75 resulted in a range of τ.

Supplemental Table 2

Contact map completeness	Number of models	Full atom RMSD<4 Å	Median RMSD [Å]	
			C_α-C_β	Full atom
100%	430	430 (100%)	0.76	2.39
90%	460	460 (100%)	0.85	2.42
70%	460	460 (100%)	1.16	2.56
50%	465	412 (89%)	2.04	3.30
30%	361	5 (1.4%)	5.95	6.87
30-100%	2176	1767 (81%)	1.14	2.61

Structural quality assessment of models based on randomly reduced contact maps.

Supplemental Table 3

Structural	Functional feature				
RMSD	$\lvert\Delta I_{in}\rvert$	$\lvert\Delta\frac{I^+_{in}}{I^-_{in}}\rvert$	$\lvert\Delta I_{out}\rvert$	$\lvert\Delta\frac{I^+_{out}}{I^-_{out}}\rvert$	$\lvert\Delta\lvert\frac{I^+_{out}}{I^+_{in}}\rvert\rvert$
general C_α-C_β	0.23	0.32	0.15	0.34	0.01
general full atom	0.24	0.31	0.13	0.32	0.02
LEU40 PRO63 GLY79 PRO83 GLY88 GLY104	0.21-0.23	0.28-0.30	0.12-0.15	0.30-0.31	-0.01-0.03
O_{GLY79} O_{ASP80}	0.22-0.23	0.29	0.12-0.14	0.31	0.01-0.02

Structural features whose Kendall's correlation with at least one functional feature was above 0.30.

Supplemental Table 4

Condition	RMSE	$Sp \cdot Sn$	Sp	Sn	ACC	MCC	$AUROC$
$\lvert\Delta\frac{I^+_{out}}{I^-_{out}}\rvert < 3.90$	< 0.3 V	0.43	0.72	0.60	0.65	0.31	0.70
$\lvert\Delta\frac{I^+_{out}}{I^-_{out}}\rvert < 4.15$	< 0.5 V	0.51	0.78	0.65	0.68	0.35	0.75
$\lvert\Delta\frac{I^+_{in}}{I^-_{in}}\rvert < 2.80$	< 0.3 V	0.44	0.83	0.53	0.65	0.36	0.71
$\lvert\Delta\frac{I^+_{in}}{I^-_{in}}\rvert < 3.60$	< 0.5 V	0.51	0.76	0.67	0.69	0.36	0.76
$\lvert\Delta I_{out}\rvert < 0.75\,\mathrm{pA}$	< 0.3 V	0.38	0.59	0.65	0.63	0.23	0.67
$\lvert\Delta I_{out}\rvert < 1.00\,\mathrm{pA}$	< 0.5 V	0.44	0.59	0.75	0.72	0.30	0.72
$\lvert\Delta I_{in}\rvert < 0.90\,\mathrm{pA}$	< 0.3 V	0.35	0.55	0.64	0.61	0.19	0.61
$\lvert\Delta I_{in}\rvert < 0.90\,\mathrm{pA}$	< 0.5 V	0.38	0.62	0.62	0.62	0.19	0.66

Optimal classification parameters based on selectivity deviation and current deviation related to electrostatic RMSE as the *ground truth*.

Supplemental Figure 1

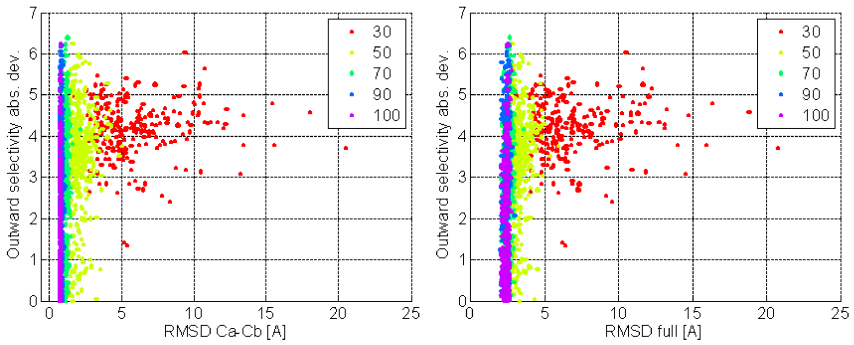

Scatter plot of general RMSD vs. absolute deviation of outward selectivity

Supplemental Figure 2

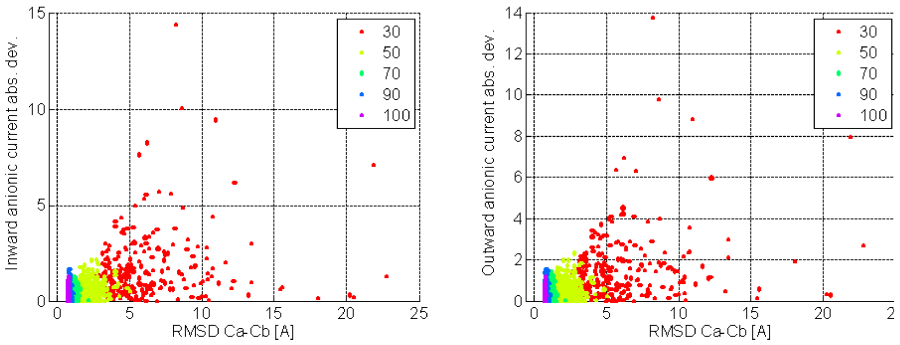

Scatter plot of general C_α-C_β RMSD vs. absolute deviation of anionic current